# Dislocations in Solids

## Volume 5

## Other Effects of Dislocations: Disclinations

*Edited by*

F. R. N. NABARRO

ISBN: Volume 1 0 7240 0756 7
Volume 2 0 444 85004 X
Volume 3 0 444 85015 5
Volume 4 0 444 85025 2
Volume 5 0 444 85050 3
Set 0 444 85269 7

Published by:
NORTH-HOLLAND PUBLISHING COMPANY
AMSTERDAM · NEW YORK · OXFORD

Sole distributors for the USA and Canada:
ELSEVIER NORTH-HOLLAND, INC.
52 VANDERBILT AVENUE
NEW YORK, N.Y. 10017

**Library of Congress Cataloging in Publication Data**

Main entry under title:

Dislocations in solids.

Includes bibliographies and indexes.
CONTENTS: v. 1. The elastic theory.—[etc.]—
v. 5. Other effects of dislocations: disclinations.
1. Dislocations in crystals—Collected works.
2. Solid state physics—Collected works. I. Nabarro, Frank Reginald Nunes, 1916-
QD921.D55 548'.842 78-10507
ISBN 0-444-85269-7 (set)

Printed and bound in Great Britain by
William Clowes (Beccles) Limited, Beccles and London

# Preface

The chapters in this volume fall into two groups. The first group treats the influence of ordinary translational dislocations on phenomena which tend to interest physicists rather than metallurgists; the second group treats the theory and properties of rotational dislocations – disclinations.

In Chapter 18, C. J. Humphreys describes the many methods of obtaining images of the dislocations in a crystal, using beams of electrons, X-rays or visible light, or by field-ion emission. The next chapter, by B. Mutaftschiev, shows the very great influence which dislocations may have on the rate of crystal growth, and the way in which the mechanisms of crystal growth lead to the multiplication of dislocations. In Chapter 20, R. Labusch and W. Schröter discuss the electrical effects of dislocations in semiconductors of the diamond and sphalerite structures, effects which can be of great technical importance. The last chapter in this group, by F. R. N. Nabarro and A. T. Quintanilha, treats the motion of lattice dislocations in a superconducting metal, the interaction between lattice dislocations and flux lines in a Type II superconductor, and dislocations in the flux-line lattice.

In the second group, M. Kléman develops in Chapter 22 the general theory of disclinations, with applications to solid crystals and nematic and cholesteric liquid crystals. This theoretical study is followed by an account by Y. Bouligand of the defects and textures which are observed in liquid crystals of the smectic, myelinic, cholesteric and nematic classes, and their interpretation in terms of disclinations. Finally, M. Kléman describes the relation between magnetoelasticity and dislocation theory, the singularities which appear in spin lattices, and the interactions of lattice dislocations with the magnetic structure of a ferromagnetic crystal.

F. R. N. Nabarro

# Contents

Volume 5.

CHAPTER 18

# Imaging of Dislocations

C. J. HUMPHREYS

*Department of Metallurgy and Science of Materials*
*University of Oxford*
*Oxford, UK*



*Dislocations in Solids*
*Edited by F. R. N. Nabarro*

# Contents

## 1. *Introduction*

This chapter will concentrate on the most important techniques for the imaging of dislocations and in particular upon significant recent developments which have not yet been reviewed in other publications. There are a number of such recent advances, notably in transmission electron microscopy, scanning electron microscopy, high-voltage electron microscopy, field-ion microscopy, X-ray topography, and optical microscopy, which will be reviewed here for the first time. Early developments, up to 1964, have been well covered in the book by Amelinckx [1].

The general scheme adopted for describing a particular imaging technique will be to give first a simple qualitative physical explanation of the method and the theory, followed by some experimental results and then a more detailed treatment. The emphasis throughout will be on interpreting image structure in terms of object structure, and the approximations and assumptions normally made will be assessed.

Section 2 discusses transmission electron microscopy. The theory and principles of electron propagation in crystals are presented in some detail since this forms the basis not only of sect. 2 but also of sects. 3 and 4. For accuracy and generality the many-beam dynamical theory of electron diffraction is used. Included in sect. 2 is a description of conventional imaging techniques, the effects of anisotropic elasticity on dislocation images, the weak-beam technique, the interpretation of lattice images and a discussion of computed micrographs.

High-voltage electron microscopy is considered in sect. 3, which contains an assessment of the advantages of using higher voltages, a comparison of different high-resolution imaging methods, the use of environmental cells and in-situ dynamic experiments. Both scanning transmission and scanning reflection electron microscopy are described in sect. 4 with applications to imaging defects in both thin and bulk specimens. Bulk specimens are also considered in sect. 5, which deals with X-ray topographic methods. Sections 6 and 7 briefly consider recent developments in field-ion and optical microscopy respectively.

## 2. *Transmission electron microscopy*

### 2.1. Conventional diffraction contrast methods

#### *2.1.1. Principles*

The basic principles of the electron microscope are well-known (see, for example, Hirsch et al. [2]) and hence will only be briefly summarised here. The electron microscope is essentially analogous to the optical microscope except that the incident radiation is a beam of electrons rather than a beam of light and the focussing lenses are electromagnetic rather than optical. In a conventional electron microscope the incident electrons typically have an energy of 100 keV, corresponding to a wavelength

of 0.037 Å: thus the resolution set by diffraction is of this order. In practice the instrumental resolution is limited by lens aberrations and is typically a few Å in favourable cases. If the specimen is crystalline the scattered electrons are concentrated in discrete directions, corresponding to Bragg reflection directions, and these electrons are brought to a focus in the focal plane of the objective lens, i.e. the diffraction pattern is formed in this plane. An aperture (the objective aperture) may be inserted in this plane to select only one spot of the diffraction pattern. The electrons in this spot pass through the aperture to form an image in the image plane of the lens. Additional lenses are normally used to provide further magnification up to about 500,000 times. If the objective aperture selects the spot formed by the directly transmitted beam, the corresponding image is known as the bright-field image. If the image is formed using a diffracted beam the image is called a dark-field image. Electrons are relatively strongly inelastically scattered by solids and hence only fairly thin specimens can be studied by transmission electron microscopy. Typical maximum usable specimen thicknesses range from about 1 $\mu$m for light materials (e.g. aluminum) down to less than 1000 Å for heavy materials (e.g. uranium). However, if a high-voltage electron microscope is used, thicker specimens may be penetrated (see sect. 3.1). The specimen is normally oriented at or near a low-order Bragg position so that only one diffracted beam is strong: this is the so-called "two-beam condition" (i.e. the direct beam plus one diffracted beam).

If the crystalline specimen were completely free of defects, unbent and of uniform thickness, then the bright-field or dark-field image would be of uniform intensity. However if the crystal contains a dislocation, the lattice planes are locally distorted and hence diffract electrons differently from perfect regions of crystal. Thus dislocations may be imaged in bright or dark field, the image corresponding to the local change in diffracted intensity produced by the distortion of the lattice planes. This conventional method of imaging is known as diffraction contrast, and dislocations were first imaged by this method in 1956 by Hirsch et al. [3] and independently by Bollmann [4].

It follows from the above qualitative description that if the Bragg reflecting planes operating are not distorted by the dislocation, then there will be no change in the diffracted intensity, i.e. the dislocation will be invisible in the image. For example, for a screw dislocation in an isotropic medium planes parallel to the axis remain flat. Hence if the diffraction vector $\boldsymbol{g}$ is perpendicular to the Burgers vector $\boldsymbol{b}$ no image contrast is observed. Thus a screw dislocation is invisible if $\boldsymbol{g} \cdot \boldsymbol{b} = 0$, and this criterion can be used to determine the direction of $\boldsymbol{b}$ by finding two sets of planes, $\boldsymbol{g}_1$ and $\boldsymbol{g}_2$, for which the invisibility criterion is satisfied: $\boldsymbol{b}$ is then parallel to $\boldsymbol{g}_1 \times \boldsymbol{g}_2$.

It is possible to account for many of the features of dislocation images by using simple qualitative arguments similar to the one used above. However, a detailed quantitative interpretation of dislocation images is often necessary, for which an accurate theory is required. The first attempt at this, based on the kinematical theory of electron diffraction (Hirsch et al. [5]), is useful for qualitatively explaining various image contrast features. The kinematical theory of electron diffraction assumes that the amplitude diffracted by a crystal is proportional to the Fourier transform of the crystal. The theory is analogous to the use of Fourier transforms in optical diffraction

theory in which the scattered amplitude in Fraunhofer diffraction is proportional to the Fourier transform of the object. It is also analogous to the first Born approximation in quantum mechanics in which the scattered amplitude is proportional to the Fourier transform of the scattering potential. All of these single-scattering approximations are valid only if the scattered amplitude is weak. This is normally the case in optics, it is often the case in quantum mechanical scattering problems (see standard quantum mechanics texts for a discussion of the validity of the Born approximation): it is, however, only rarely the case in electron diffraction. If a crystal is set at a low-order Bragg reflecting position, the intensity of the Bragg diffracted beam reaches one tenth of the intensity of the incident beam for a crystal thickness of typically only 20 Å for 100 kV electrons, and the intensities of the transmitted and the diffracted beams are equal for thicknesses of typically 60 Å. Hence the kinematical theory is invalid for crystals more than a few atoms thick which are oriented near to a Bragg position. If the crystal is far from a Bragg position and the diffracted beam or beams are weak, the kinematical theory may then be valid as a first approximation (see sect. 2.2 on the weak-beam technique). However due to its very limited quantitative use the kinematical theory will not be discussed further here. The fact that single-scattering Fourier transform theories are not normally valid in the electron microscopy of crystals is not always appreciated, and has caused, and still causes, considerable confusion, particularly in the interpretation of lattice images of crystals containing defects (sect. 2.3).

As emphasised above, in most applications of electron microscopy at least one diffracted beam is strong, the kinematical theory cannot be used and instead a dynamical theory is necessary, that is a theory which takes into account multiple scattering of, and coupling between, the various diffracted beams. Several formulations of a dynamical theory exist (e.g. Bethe [6], Cowley and Moodie [7], Howie and Whelan [8]) which are all mathematically equivalent. The formulation that will be used throughout this chapter is based on that of Bethe [6], and represents the wave function for fast electrons within the crystal as a linear superposition of Bloch waves. In order to understand image contrast effects from defects it is first necessary to consider electron propagation in a perfect crystal which is discussed below, defect contrast being considered in sect. 2.1.3.

### *2.1.2. Diffraction by perfect crystals*

The basic theory and some applications will be outlined in this section. For a fuller discussion see, for example, Hirsch et al. [2] or Cowley [9]. Since 100 keV electrons have a velocity $v = 0.55\ c$ (where $c$ is the velocity of light) it would seem that the diffraction problem requires the solution of the Dirac equation. However the effects of electron spin are usually negligible (Fujiwara [10]) and the problem reduces to solving the Schrödinger equation for the system of the incident fast electron and the crystal, provided that relativistically correct values for the electron mass and wavelength are used. It is perhaps worth noting that electron diffraction theory is essentially similar to band theory except that in electron diffraction the incident electron energy is fixed and positive and the basic problem is to find permitted values of the electron wave vector inside the crystal: in band theory the problem is to find permitted values

of the electron energy (negative corresponding to bound states) for given values of the wave vector (see Humphreys and Fisher [11]).

The Schrödinger equation for the fast electron within the crystal potential $V(\boldsymbol{r})$ is

$$\nabla^2\psi(\boldsymbol{r}) + (8\pi^2 m|e|/h^2)\,[E + V(\boldsymbol{r})]\psi(\boldsymbol{r}) = 0, \tag{1}$$

where $\psi(\boldsymbol{r})$ is the wave function and $m$ the (relativistic) mass of the fast electron. $E$ is the incident electron accelerating potential (so that the total energy of the incident electron is $|e|E$), and $V(\boldsymbol{r})$ is the crystal lattice potential, defined here as being intrinsically positive since the incident electrons are attracted by the atoms.

Within the perfect crystal the periodic potential may be expanded as a Fourier series based on the reciprocal lattice,

$$V(\boldsymbol{r}) = \sum_{-\infty}^{\infty} V_{\boldsymbol{h}} \exp(2\pi i \boldsymbol{h}\cdot\boldsymbol{r}). \tag{2}$$

(Throughout this chapter reciprocal space quantities are defined as true reciprocals of real space quantities.)

The electron wave function within the crystal may in general be represented by a linear combination of Bloch waves,

$$\psi(\boldsymbol{r}) = \sum_j A^{(j)} b^{(j)}(\boldsymbol{k}^{(j)}, \boldsymbol{r}). \tag{3}$$

Each Bloch wave is the product of a plane wave $\exp(2\pi i \boldsymbol{k}^{(j)}\cdot\boldsymbol{r})$ and a function $C(\boldsymbol{r})$ which has the periodicity of the lattice. We may expand $C(\boldsymbol{r})$ as a Fourier series based on the reciprocal lattice to give

$$b^{(j)} = \sum_{\boldsymbol{g}} C_{\boldsymbol{g}}^{(j)} \exp[2\pi i(\boldsymbol{k}^{(j)} + \boldsymbol{g})\cdot\boldsymbol{r}]. \tag{4}$$

The constants may be collected together by defining a "modified potential" $U(\boldsymbol{r})$ with Fourier coefficients

$$U_{\boldsymbol{h}} = (2m|e|/h^2)V_{\boldsymbol{h}} \tag{5}$$

and a quantity $K$ given by

$$K^2 = (2m|e|/h^2)(E + V_0) \tag{6}$$

where $K$ is the magnitude of the mean electron wave vector within the crystal after allowing for the mean crystal potential (a small correction: typically $E = 10^5$ volts, $V_0 \leqslant 10$ volts).

Substituting eqs. (2) to (6) in eq. (1) and equating the coefficient multiplying each exponential term separately to zero yields the set of linear equations

$$[K^2 - (\boldsymbol{k}^{(j)} + \boldsymbol{g})^2]C_{\boldsymbol{g}}^{(j)} + \sum_{\boldsymbol{h}\neq 0} U_{\boldsymbol{h}} C_{\boldsymbol{g}-\boldsymbol{h}}^{(j)} = 0, \tag{7}$$

there being one such equation for each value of $\boldsymbol{g}$ (i.e. each reflection) considered.

In the two-beam approximation, for example, there are two equations each consisting of two terms as follows:

$$(K^2 - k^{(j)2})C_0^{(j)} + U_{-g}C_g^{(j)} = 0$$
$$U_g C_0^{(j)} + [K^2 - (\boldsymbol{k}^{(j)} + \boldsymbol{g})^2]C_g^{(j)} = 0. \tag{8}$$

The two-beam approximation is normally valid as a first approximation for 100 kV microscopy when the crystal is oriented at or near a first-order Bragg reflecting position, since for most simple structures the $U_g$ values decrease fairly rapidly with increasing $|\boldsymbol{g}|$, and at 100 kV $|C_0^{(j)}|$ and $|C_g^{(j)}|$, for $j = 1$ and 2, are normally much larger than the other coefficients (the two-beam approximation breaks down however for higher incident electron energies, see sect. 3).

Equation (8) has a solution if the determinant of the coefficients vanishes i.e. if

$$\begin{vmatrix} K^2 - k^{(j)2} & U_{-g} \\ U_g & K^2 - (\boldsymbol{k}^{(j)} + \boldsymbol{g})^2 \end{vmatrix} = 0. \tag{9}$$

In the many-beam case, if $n$ values of $\boldsymbol{g}$ are considered in eq. (7) (i.e. the $n$-beam case), then (9) becomes an $n \times n$ determinant, each diagonal term involving $k^{(j)2}$, so that the determinant is an equation in $k^{(j)2n}$, there being $n$ positive and $n$ negative roots, corresponding to forward and backward propagation respectively. At high energies in transmission electron microscopy the backward propagating waves are only produced by "reflection" at the lower surface of the crystal. Application of the boundary conditions shows that these reflected waves have extremely small intensity, hence essentially if $n$ beams are considered, there are $n$ different values of the electron wave vector within the crystal for a particular orientation of the crystal with respect to the beam.

Physically, the crystal acts as its own interferometer. An incident electron of fixed energy $|e|E$ and fixed wave vector is partitioned by the crystal into a set of Bloch waves of differing wave vectors $\boldsymbol{k}^{(j)}$. As each Bloch wave propagates it becomes out of phase with its neighbors (due to its different wave vector). If the crystal is wedge-shaped, interference fringes called thickness fringes occur.

If $n$ beams are considered there are $n$ positive values of $\boldsymbol{k}^{(j)}$ for a given orientation of the crystal with respect to the incident beam. For a different orientation the $n$ permitted values of $\boldsymbol{k}^{(j)}$ are different. A plot of the permitted values of $k_z^{(j)}$, the component of $\boldsymbol{k}^{(j)}$ normal to $\boldsymbol{g}$, as a function of orientation, is known as a dispersion surface, and is illustrated in fig. 1. If $n$ beams are considered then the dispersion surface has $n$ branches corresponding to the $n$ values of $k_z^{(j)}$. The numbering system used for labelling these branches and the corresponding Bloch waves has been a subject of some confusion. Prior to about 1971, the system normally used in publications was to label the top branch of the dispersion surface (i.e. the branch with the highest $k_z^{(j)}$ value) branch 2 and the next branch 1. There was then some confusion over whether the branch with the third largest $k_z^{(j)}$ value was labelled 3 or 4, some publications choosing 3 and some 4. Since about 1971 most publications have used an ordered labelling scheme (Humphreys and Fisher [11]) which numbers the dispersion surface branches from the upper to the lower, i.e. 1, 2, 3, 4, etc. in order of

decreasing $k_z$. This scheme will be used throughout this chapter. Apart from its simplicity the scheme has the advantage of being consistent with band theory and lattice vibration theory.

Values of the Fourier coefficients of the modified potential $U_g$ may be obtained from tabulated values of atomic scattering factors (see Hirsch et al. [2] for details) and hence the 2-beam-approximation equations (8) may be solved by hand, or the many-beam equations (7) may be solved by a computer to yield the values of the wave vectors $\boldsymbol{k}^{(j)}$ and of the Bloch wave coefficients $C_g^{(j)}$.

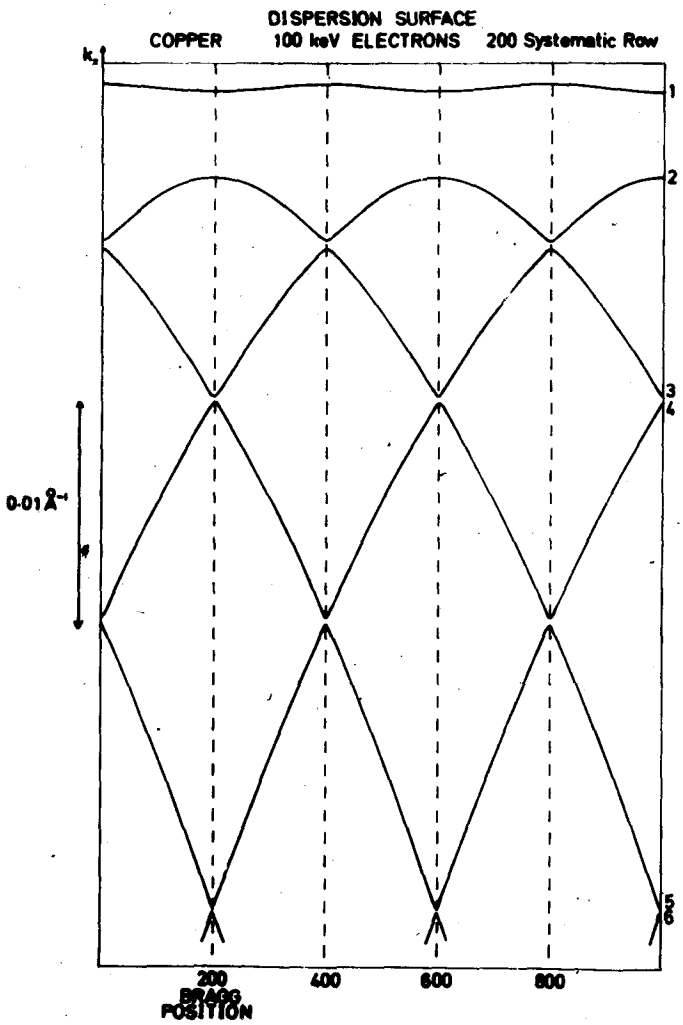


Fig. 1 Calculated dispersion surface for 100 keV electrons incident upon copper at 300 K. The many-beam calculations take into account 20 reflections along the 200 systematic row.

The Bloch waves given by eqs. (3) and (4) propagate to the bottom surface of the crystal, where they decompose into their plane wave components. From eqs. (3) and (4), the amplitude in the $g$th diffracted beam leaving the crystal is

$$v_g = \sum_j^i A^{(j)} C_g^{(j)} \exp\left[2\pi i(\boldsymbol{k}^{(j)} + \boldsymbol{g})_t t\right], \tag{10}$$

where $t$ is the crystal thickness and $(\boldsymbol{k}^{(j)} + \boldsymbol{g})_t$ represents the component of $(\boldsymbol{k}^{(j)} + \boldsymbol{g})$ in a direction parallel to $t$. In the symmetric Laue case (i.e. when the diffracting planes are perpendicular to the surface, which is normally approximately the case in transmission electron microscopy) application of the boundary conditions shows that $A^{(j)} = C_0^{(j)}$ (see Hirsch et al. [2]). Hence the intensity diffracted in the $g$th beam is

$$I_g = \left| \sum_j A^{(j)} C_g^{(j)} \exp\left(2\pi i k^{(j)} t\right) \right|^2, \tag{11}$$

where by $k^{(j)}$ is now understood the component of $\boldsymbol{k}^{(j)}$ parallel to $t$, which in the symmetric Laue case is $k_z^{(j)}$ ($z$ perpendicular to $\boldsymbol{g}$).

If only one diffracted beam is strong and 2-beam theory is used, it follows from eq. (11) that the intensity of the direct beam $I_0$ is proportional to $\cos^2(\pi t \Delta k)$ and the intensity of the diffracted beam $I_g$ is proportional to $\sin^2(\pi t \Delta k)$, where $\Delta k = k^{(1)} - k^{(2)}$. Thus for a wedge-shaped crystal $I_0$ and $I_g$ both oscillate with thickness producing the well-known "thickness fringes". Intensity is conserved ($\sin^2 + \cos^2 = 1$) for all $t$ as expected since absorption has not yet been included in the theory. The fringe spacing is a maximum when $\Delta k$ is a minimum, which corresponds to the crystal being at an exact Bragg position (see fig. 1). The extinction distance $\xi_g'$ is defined as

$$\xi_g = \frac{1}{\Delta k_{\min}} = \frac{1}{(k^{(1)} - k^{(2)})_{\min}}.$$

The diffracted beam has minimum intensity for $t = m\xi_g$ where $m$ is an integer.

So far only elastic scattering has been considered. Inelastic scattering causes electrons not only to lose energy but also to be angularly scattered out of the Bragg beams. The objective aperture selects one of the Bragg beams to form the image, and hence many of the inelastically scattered electrons are excluded from the image. Thus inelastic scattering produces absorption. The effects of absorption may be simply taken into account in the above theory by making the crystal potential and the electron wave vectors complex. A justification for this phenomenological treatment has been given by Yoshioka [12] (see also Hashimoto et al. [13]).

Hence

$$\boldsymbol{k}^{(j)} \to \boldsymbol{k}^{(j)} + i\boldsymbol{q}^{(j)}. \tag{12}$$

It follows from the boundary conditions that the direction of $\boldsymbol{q}$ is along the inward surface normal, hence the total electron wave function in the crystal is (using eqs. (3) and (4))

$$\psi(\boldsymbol{r}) = \sum_j A^{(j)} \exp\left(-2\pi q^{(j)} z\right) \sum_g C_g^{(j)} \exp\left[2\pi i(\boldsymbol{k}^{(j)} + \boldsymbol{g}) \cdot \boldsymbol{r}\right]. \tag{13}$$

The effect of absorption is thus to attenuate each Bloch wave exponentially, as is physically expected. In the absence of absorption, each Bloch wave excitation amplitude in the crystal $A^{(j)}$ is a constant ($= C_0^{(j)}$, from the boundary conditions at the top surface of the crystal). The effect of absorption is to replace $A^{(j)}$ by an exponentially attenuated amplitude $A^{(j)}(z)$, where

$$A^{(j)}(z) = A^{(j)} \exp(-2\pi q^{(j)} z) \tag{14}$$

and the origin of $z$ is taken on the top surface of the crystal.

The intensity of the $g$th diffracted beam is, from eqs. (11) and (12),

$$I_g = |\sum_j A^{(j)} C_g^{(j)} \exp(2\pi i k^{(j)} t) \exp(-2\pi q^{(j)} t)|^2. \tag{15}$$

The effect of absorption on the thickness fringes considered above is to produce damped fringes. Typically only about 5 fringes are visible at 100 kV in a wedge-shaped specimen of medium atomic weight.

The values of $q^{(j)}$ differ for different $j$ values, i.e. for different Bloch waves. Hence some Bloch waves are more strongly absorbed than others. This phenomenon is known as anomalous absorption (or alternatively as anomalous transmission). The physical reason for this is that each Bloch wave has a different $k^{(j)}$ value and hence a different kinetic energy. Since the total energy (kinetic plus potential) of each Bloch wave is constant (equal to the incident beam energy), the potential energies of the Bloch waves must differ, hence each Bloch wave has a different localisation within the crystal lattice. Now the main inelastic scattering mechanisms which give rise to absorption are phonon scattering and single electron excitation, and both of these processes are reasonably strongly localised at the atomic positions (particularly phonon scattering). Hence the Bloch wave which undergoes the greatest absorption is the one which is the most strongly localised at the atom planes.

The intensity of the $j$th Bloch wave is $|b^{(j)}|^2$, which may be evaluated using eq. (4) together with the values of $k^{(j)}$ and $C_g^{(j)}$. Using the 2-beam approximation, $|b^{(1)}|^2$ and $|b^{(2)}|^2$ are easily evaluated by hand. At the exact Bragg position the current in both Bloch waves is parallel to the reflecting planes. The intensity distribution in wave 1 is proportional to $\cos^2(\pi \boldsymbol{g} \cdot \boldsymbol{r})$ and in wave 2 is proportional to $\sin^2(\pi \boldsymbol{g} \cdot \boldsymbol{r})$ where the origin of $\boldsymbol{r}$ is taken at an atomic position. This is illustrated in fig. 2. Hence clearly wave 1 is strongly absorbed and wave 2 is well transmitted. This is the normal situation in 100 kV microscopy (but not necessarily at 1 MV, see sect. 3).

For thick crystals at 100 kV, for which the transmitted intensity is essentially due to wave 2 alone, eq. (15) gives for the bright-field intensity

$$I_0(t) = |C_0^{(2)}|^4 \exp(-4\pi q^{(2)} t), \tag{16}$$

since $A^{(2)} = C_0^{(2)}$. The orientation which maximises the penetration is hence that orientation for which $|C_0^{(2)}|$ is large and simultaneously $q^{(2)}$ is small. Figure 3 gives calculated many-beam plots of $C_0^{(j)}$ and $q^{(j)}$. Clearly the orientation which maximises the bright-field penetration is with the crystal oriented slightly positive of the first-order Bragg reflecting position, as is well known experimentally. This is confirmed in fig. 4 which plots the calculated transmitted intensity, for the bright-field and

several dark-field images, as a function of the angle of incidence of the electron beam for a 2000 Å thick Cu crystal. Values of absorption parameters for use in electron diffraction calculations have been given by Humphreys and Hirsch [15].

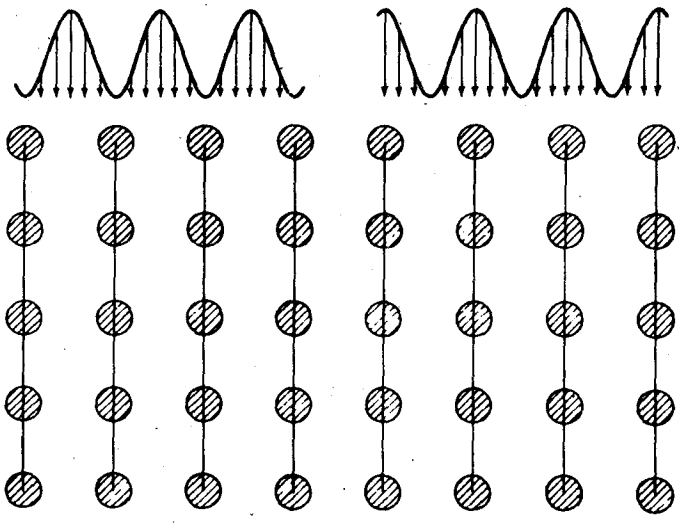

Fig. 2 The intensity distribution, relative to the Bragg reflecting planes, of Bloch waves 1 and 2 for a crystal oriented at the exact Bragg position. Wave 1 is on the right and wave 2 on the left, using the numbering scheme of ref. [11].

### *2.1.3. Diffraction by dislocations*

Dislocations produce image contrast essentially because they locally change the orientation of the lattice planes, and thus they locally change the diffracting conditions. Whereas good penetration requires the transmitted intensity $I$ to be large, good image contrast requires $\mathrm{d}I/\mathrm{d}\theta$ to be large. Fortunately the orientation which maximises the penetration using 100 keV electrons (i.e. just positive of the first-order Bragg position) is also a good orientation for defect contrast since $\mathrm{d}I/\mathrm{d}\theta$ is large here as can be seen from fig. 4. Using this figure we can obtain a qualitative idea of the amount of image contrast produced by a dislocation, by noting the change in intensity produced by a given change in orientation. This interpretation cannot be taken very far, however, since it essentially averages misorientations within a column of imperfect crystal.

Most image contrast calculations in electron microscopy are based upon the column approximation (Heidenreich [16]; Hirsch et al. [5]; Howie and Whelan [8]). In this approximation the imperfect crystal is divided into columns with the length of each column being parallel to the reflecting planes operating. The displacement in a given column is assumed to be a function of the $z$ co-ordinate only and is represented by $\boldsymbol{R}(z)$. The basic assumption of the column approximation is that each column may be chosen sufficiently narrow that the displacement within it is essentially only a function of $z$, yet sufficiently wide that an electron entering the top of the column is

not scattered out of the column during its passage through the crystal. Use of the column approximation greatly facilitates image contrast calculations since it essentially enables the problem of solving a coupled set of three-dimensional partial differential equations to be reduced to that of solving a coupled set of one-dimensional ordinary differential equations (in $z$ only), i.e. eq. (19).

Calculations for standard bright-field or dark-field images of dislocations show that in most cases the column approximation is a very good approximation (Howie and Basinski [17], Jouffrey and Taupin [18], Howie and Sworn [26]). However, for high-resolution imaging of dislocations, using for example the weak-beam technique (sect. 2.2) or lattice imaging (sect. 2.3), calculations show that the column approximation is no longer valid. The approximation also breaks down at lower resolutions if the crystal is very thick (Humphreys and Drummond [136]).

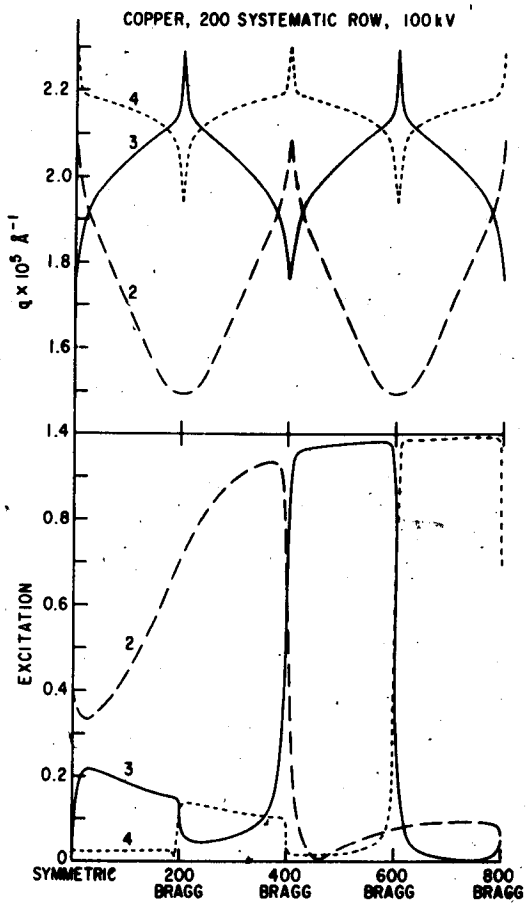


Fig 3 Computed 20-beam-theory Bloch wave absorption coefficients, $q$, and amplitude excitation coefficients for 100 keV electrons incident upon copper at 300 K, with the 200 systematic row of reflections operating. Reprinted from ref. [14], by courtesy of The Philosophical Magazine.

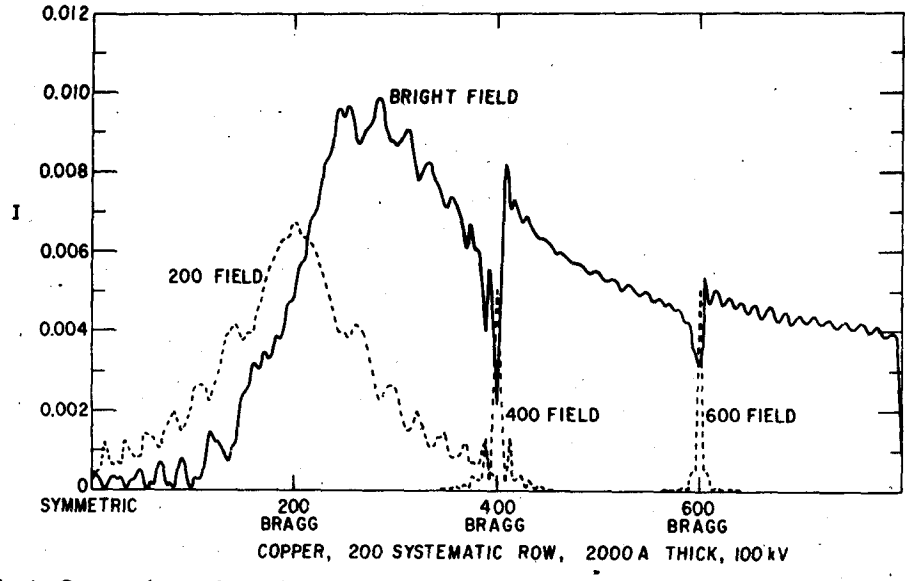


Fig. 4 Computed many-beam-theory rocking curves for 100 keV electrons incident upon copper, 2000 Å thick, 200 systematic row. Reprinted from ref. [14], by courtesy of The Philosophical Magazine.

Whereas a perfect crystal scatters into discrete, Bragg directions, an imperfect crystal scatters into all directions, and this scattering into directions other than Bragg directions is called elastic diffuse scattering. For an isolated defect the elastic diffuse scattering is peaked about the Bragg directions. The column approximation artificially constrains all of the elastic diffuse scattering to travel only in the Bragg directions, and the avoidance of the column approximation removes this constraint. If one is interested in details of defect structure, for example in dislocation core structures, it would seem in principle desirable to image using the elastic diffuse scattering itself, i.e. by placing the objective aperture between Bragg spots rather than around them. This has not yet been done owing to the experimental requirements of very high microscope stability and resolution and the theoretical difficulties of image interpretation. However, elastic diffuse imaging would appear to be a likely area of activity in the future. Such images should yield information on the atomic coordinates of the dislocation core.

At present, the deformable-ion approximation is usually used in image interpretation. Let a perfect crystal be deformed. If the $j$th atom is moved from position $\boldsymbol{r}_j$ to $\boldsymbol{r}_j + \boldsymbol{R}(\boldsymbol{r}_j)$ the potential at any point $\boldsymbol{r}$ in the crystal is clearly changed since it depends upon $\boldsymbol{r} - \boldsymbol{R}$. In the deformable-ion approximation, the potential at any point $\boldsymbol{r}$ in the deformed crystal is identified with the potential at the point $(\boldsymbol{r} - \boldsymbol{R}(\boldsymbol{r}))$ in the undeformed crystal. Hence the potential in the deformed crystal can be expanded as a Fourier series, as was done for the undeformed crystal [eq. (2)], i.e.

$$V(\boldsymbol{r}) = \sum_{-\infty}^{\infty} [V_{\boldsymbol{h}} \exp(-2\pi i \boldsymbol{h}\cdot\boldsymbol{R})] \exp(2\pi i \boldsymbol{h}\cdot\boldsymbol{r}). \tag{17}$$